Stanford Exploration Project, Report 115, May 22, 2004, pages 13–28

Adaptive phase-ray wavefield extrapolation

Jeff Shragge and Paul Sava[1]

ABSTRACT

Riemannian wavefield extrapolation (RWE) is a generalization of downward continuation to coordinate systems that closely conform to the orientation of extrapolated wavefields. If the coordinate system overturns, so does the computed wavefield, despite being extrapolated with a one-way solution to the acoustic wave-equation. This allows for accurate imaging of structures of arbitrarily steep dips with simple operators equivalent to standard 15° extrapolators. An obvious question for RWE is which is an optimal coordinate system for a given velocity model. One option is to compute ray coordinates as a solution to the wide-band eikonal equation in a smoothed velocity model. However, this solution ignores the natural variability and frequency dependence of wavepaths in cases of complicated velocity models, for example under salt bodies. The solution advocated in this paper is a recursive bootstrap procedure where a frequency-dependent coordinate system is computed on-the-fly at every step from the gradient of the monochromatic wavefield phase of the preceding few steps, coupled with standard RWE.

INTRODUCTION

Wavefield extrapolation extends surface-recorded data to depth through application of a wave-equation operator. The choice of operator depends mainly on practical considerations (e.g. computer memory, total flop count); however, one persistent theoretical constraint is the degree of velocity model complexity. In laterally invariant media, closed-form Fourier-domain operators (single square root, SSR) can accurately extrapolate surface recorded wavefields up to 90° (Gazdag, 1978; Claerbout, 1985). However, such solutions are inapplicable in media characterized by lateral velocity variation, and approximate solutions to the SSR equation are employed. Consequently, the accuracy of the extrapolation operators degrades, particularly at high angles relative to the downward extrapolation axis, and more sophisticated procedures are required to ensure wavefield accuracy.

Improved wavefield extrapolation can be achieved in many ways. First, one may improve the high-angle accuracy of an operator while retaining a Cartesian computational grid. Examples of this include incorporating higher-order terms in the expansion of Fourier domain operators (e.g. Fourier finite-difference (Ristow and Ruhl, 1994), generalized screen propagator (de Hoop et al., 2000)), or using tilted Cartesian coordinate systems (Zhang and McMechan,

[1]**email:** jeff@sep.stanford.edu, paul@sep.stanford.edu

1997; Etgen, 2002; Shan and Biondi, 2004) that extend the accuracy of high-angle propagation. Second, seismic wavefields may be spatially partitioned into more manageable sections and then independently extrapolated in preferred directions. For example, decomposing data sections to form local beams for extrapolating along tubes of finite thickness (Hill, 2001; Albertin et al., 2001; Gray et al., 2002; Brandsberg-Dahl and Etgen, 2003).

A third option is to abandon the strictures of Cartesian coordinates altogether and represent the physics of one-way wavefield extrapolation in a generalized coordinate system that obeys the tenets of differential geometry (Guggenheimer, 1977). In particular, one could use a basis (or coordinate system) that conforms to where the wavefronts propagate (Sava and Fomel, 2004). In this reference frame low-angle operators remain applicable, and the extrapolation procedure is of high fidelity, even at arbitrarily large angles to depth axis. The strategy espoused in this paper is the latter: it is more prudent to adjust the coordinate system to conform better with the physics than to force the physics to work in Cartesian coordinates, or on an *a priori* spatial partition of the data or model space.

One judicious choice of non-Cartesian coordinate system is a basis derived from a suite of rays. In this approach, the natural wavefield extrapolation direction is travel-time along a ray, with orthogonal coordinates directed across the rayfront at a constant time step. However, unlike for Cartesian coordinates, the distance between adjacent rays may freely expand or contract according to the lateral variations in the velocity model. Thus, properly defining the coordinate metric requires additional parameters that account for the Jacobian-like coordinate spreading. Given a rayfield and the associated Jacobian parameters, the solution to the corresponding one-way acoustic wave-equation is generated in an ordinary fashion (Sava and Fomel, 2004). The ray-coordinate wavefield solution is then interpolated back to a Cartesian mesh through a simple mapping operation.

One of the practical difficulties of ray-coordinate-based wavefield extrapolation is developing a robust procedure for handling triplicating rayfields that naturally arise due to wavefield multipathing. In particular, we need to prevent numerical instabilities from arising when calculating coordinate Jacobian spreading and related parameters that require computing finite-difference derivatives at the ray-crossing locations. Sava and Fomel (2004) apply a regularization parameter that prevents division by zero. This procedure, though, can lead to anomalous extrapolation amplitudes, which motivates us to seek out new methods for calculating rayfields and circumventing the ubiquitous problem of ray-coordinate triplication.

Underlying ray-coordinate systems may be generated by assuming that the rayfield is frequency-independent, and computing the solution to the wide-band eikonal equation (Červený, 2001). However, this approximation can be inappropriate for complex geology where a stationary ray-coordinate system inadequately describes monochromatic wave propagation over a range of frequencies. One example is the significant frequency-dependence of rayfield illumination across salt-sediment interfaces characterized by large impedance contrasts and rugose topography. Hence, an important question is how does one expect to maintain a sufficient and consistent wavefield illumination when the underlying rayfield is itself strongly dependent on frequency? Hence, a frequency-dependent ray-coordinate systems should be an invaluable tool for enhancing imaging practice in complex media.

This paper presents a procedure for constructing a frequency-dependent ray-coordinate system in an adaptive manner directly from the wavefield. The key idea is that the rayfront vectors at any given step are directly calculable from the phase-gradient of previous wavefield solution steps. This naturally leads to a bootstrapping procedure where one alternates between calculating the coordinate system for the next step, and the corresponding wavefield solution at that step. The methodology is similar to the *Riemannian wavefield extrapolation* (RWE) technique presented by Sava and Fomel (2004), where rayfields are traced through a smoothed velocity model using a Huygens' wavefront tracer (Sava and Fomel, 2001). The method differs, though, in that frequency-stationarity of the rayfield is not assumed, and the rayfield is instead calculated on-the-fly from the monochromatic wavefield. This method also differs from Shragge and Biondi (2003) in that an initial wavefield is not required as a precondition for solution. Also included in this report is a companion paper, (Shragge and Biondi, 2004), that discusses the strategy of using wavefield solutions precomputed on a background velocity model to train an updated ray-coordinate system using phase-rays.

We begin this paper with a review of phase-ray theory, frequency-dependent coordinate system generation, and ray-coordinate wavefield extrapolation. Then, we introduce the bootstrap procedure by which the ray-coordinate system and accompanying wavefield solutions are computed. Next, we show examples of wavefields extrapolated in adaptive phase-ray coordinates, and conclude with a discussion of the complications posed by triplicating coordinate systems. A more general formulation involving the oriented wave equation (Fomel, 2003) has the potential to address this problem in a robust theoretical framework, although such opportunity remains subject to future research.

THEORY

Phase-rayfields

A monochromatic acoustic wavefield, $\mathcal{U}$, at frequency, ω, and spatial location, $\mathbf{x}$, may be represented by,

$$\mathcal{U}(\mathbf{x},\omega) = A(\mathbf{x},\omega)\,\mathrm{e}^{\mathrm{i}\phi(\mathbf{x},\omega)}, \tag{1}$$

where $A(\mathbf{x},\omega)$ and $\phi(\mathbf{x},w)$ are the amplitude and phase functions, respectively. For monochromatic waves propagating through isotropic media, the gradient of phase function, $\nabla\phi(\mathbf{x},w)$, represents the instantaneous direction of energy transport and is a characteristic to the solution of the governing Helmholtz equation (Foreman, 1989). Analogous to the ray precept in broadband theory, this vector quantity defines the instantaneous direction and magnitude of one ray in a continuous ray manifold. However, to differentiate between the broadband and monochromatic ray representations, we term the latter quantity phase-rays (Shragge and Biondi, 2003). The governing differential equations for a phase-ray, r_i, are presented in the Exact-ray formulation of Foreman (1989). In Cartesian coordinates, the subscript i on r refers to the projection of the ray along the x and z axes - r_x and r_z, respectively. The phase-ray

equations, in summation notation, are,

$$\frac{\mathrm{d}r_i}{\mathrm{d}s} = \frac{\partial \phi}{\partial x_i}\left[\left(\frac{\partial \phi}{\partial x_k}\right)\left(\frac{\partial \phi}{\partial x_k}\right)\right]^{-\frac{1}{2}}, \tag{2}$$

where ϕ is the above phase function, x_i is a coordinate of the underlying Cartesian grid, and the repeated index k here (and throughout the paper) represents a summation over all coordinate indices. Scalar step magnitude, $\mathrm{d}s$, is given by,

$$\mathrm{d}s(\mathbf{x}) = v(\mathbf{x})\,\mathrm{d}\tau, \tag{3}$$

where $v(\mathbf{x})$ is the velocity in the neighborhood of ray, $r_i(\mathbf{x})$, and $\mathrm{d}\tau$ is an element of time along the ray.

Calculating phase-rays thus requires isolating the gradient of the monochromatic phase function. An efficient procedure is to calculate the ratio of the wavefield gradient to the wavefield itself,

$$\frac{\nabla \mathcal{U}}{\mathcal{U}} = \frac{\nabla A}{A} + \mathrm{i}\nabla\phi, \tag{4}$$

which eliminates the oscillatory nature of the wavefield. Taking the imaginary component of equation (4),

$$\nabla\phi = \Im\left(\frac{\nabla \mathcal{U}}{\mathcal{U}}\right), \tag{5}$$

yields the required phase gradient. The right hand side of equation (5) is calculable only when a wavefield solution is known. The solution for a ray, r_i, is computed through integrating the right hand sides of equations (2) using a one-sided, non-stiff integration method (e.g. Simpson's 1/3 rule). Interestingly, ray solutions are uniquely determined given an initial starting position by reason that equations (2) form a decoupled system of differential equations of first-order. Accordingly, a phase-ray coordnate system is uniquely defined by specifying of a set of initial coordinate points and a frequency, ω. Note that this specification makes the coordinate system frequency dependent. Additional information on the theory of phase-rays is discussed in both Shragge and Biondi (2003) and Foreman (1989).

Ray-coordinate wavefield extrapolation

Wavefield extrapolation in ray-coordinates requires casting the acoustic wave-equation not in the usual Cartesian representation, but rather in a system parameterized by phase-ray variables. In 2-D, these variables consist of τ, the one-way travel time from a source/receiver point along the direction of a ray, and γ, the direction across the rayfront at a constant time step. A cartoon illustrating ray-coordinate geometry is presented in Figure 1.

Note that the dimensions of time and space coordinates τ and γ are seconds and meters, respectively.

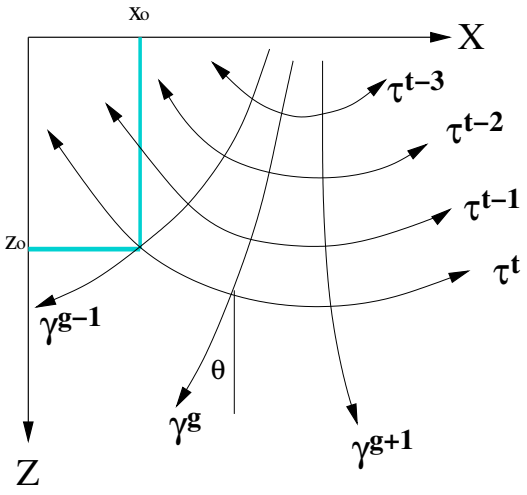

Figure 1: Cartoon illustrating the phase-ray coordinate system and its relation to the Cartesian basis. Variable $\tau = \tau(x,z)$ is the direction along a single ray, and parameter τ^t is an isochron or rayfront. Variable $\gamma = \gamma(x,z)$ is the coordinate across the rayfront at a constant τ step, and parameter γ^g is a ray. Grey lines illustrate the mapping between ray point (τ^t, γ^{g-1}) and Cartesian point (x_o, z_o). Angle θ is a rotation angle between the ray and the z-axis (assumed to be positive downward). jeff1-raycoord [NR]

The 2-D acoustic wave-equation for wavefield, $\mathcal{U}$, at frequency, ω, in ray-coordinates is (Sava and Fomel, 2003),

$$\frac{1}{vJ}\left[\frac{\partial}{\partial\tau}\left(\frac{J}{v}\frac{\partial\mathcal{U}}{\partial\tau}\right)+\frac{\partial}{\partial\gamma}\left(\frac{v}{J}\frac{\partial\mathcal{U}}{\partial\gamma}\right)\right]=-\frac{\omega^2}{v^2}\mathcal{U}, \tag{6}$$

where v is the velocity function, and J is the ray-coordinate Jacobian or geometrical ray spreading factor given by,

$$J=\left[\frac{\partial x_k}{\partial\gamma}\frac{\partial x_k}{\partial\gamma}\right]^{\frac{1}{2}}. \tag{7}$$

Importantly, parameter J is solely a component of ray-coordinates and is independent of wavefield extrapolated on the coordinate system.

Analogous to wave-equation extrapolation in Cartesian coordinates, a dispersion relation must be specified that forms the basis for all derived ray-coordinate extrapolation operators. The relation being sought is the wavenumber along the ray direction, k_τ. Following Sava and Fomel (2003), the partial derivative operators in equation (6) are expanded out to generate a second-order partial differential equation with non-zero cross derivatives. Fourier-domain wavenumbers are then substituted for the partial differential operators acting on wavefield, $\mathcal{U}$, and the quadratic formula is applied to yield the expression for k_τ,

$$k_\tau=\frac{\mathrm{i}v}{2J}\frac{\partial}{\partial\tau}\left(\frac{J}{v}\right)\pm\left[\omega^2-\left[\frac{v}{2J}\frac{\partial}{\partial\tau}\left(\frac{J}{v}\right)\right]^2+\frac{\mathrm{i}v}{J}\frac{\partial}{\partial\gamma}\left(\frac{v}{J}\right)k_\gamma-\frac{v^2}{J^2}k_\gamma^2\right]^{\frac{1}{2}}. \tag{8}$$

Note, again, that quantity $\frac{J}{v}$ depends solely on the coordinate system and is independent of the wavefield being propagated.

One relatively straightforward manner to apply wavenumber k_τ in an extrapolation scheme is to develop the ray-coordinate equivalent of Claerbout's classic 15° equation (Claerbout, 1985). This involves a second-order Taylor series expansion of the radical in equation (8), and the identification of Fourier dual parameters k_τ and k_γ with their space domain derivative counterparts $-\mathrm{i}\frac{\partial}{\partial\tau}$ and $-\mathrm{i}\frac{\partial}{\partial\gamma}$. The ray-coordinate formula corresponding to the 15° equation is,

$$\begin{aligned}\frac{\partial \mathcal{U}}{\partial \tau} \approx & - \frac{v}{2J}\frac{\partial}{\partial\tau}\left(\frac{J}{v}\right) + \mathrm{i}\omega_o + \frac{\mathrm{i}v}{2\omega_o J}\frac{\partial}{\partial\gamma}\left(\frac{v}{J}\right)\frac{\partial \mathcal{U}}{\partial\gamma} \\ & + \frac{-\mathrm{i}}{2\omega_o}\left[\left(\frac{v}{2J\omega_o}\frac{\partial}{\partial\gamma}\left(\frac{v}{J}\right)\right)^2 - \frac{v^2}{J^2}\right]\frac{\partial^2 \mathcal{U}}{\partial\gamma^2}, \end{aligned} \tag{9}$$

where ω_o may be considered as the effective (non-stationary) frequency,

$$\omega_o = \omega\left[1 - \left(\frac{v}{2\omega J}\frac{\partial}{\partial\tau}\left(\frac{J}{v}\right)\right)^2\right]^{\frac{1}{2}}. \tag{10}$$

Equation (9) may be solved in 2-D using fully implicit finite difference methods (e.g. Crank-Nicolson) and fast tridiagonal solvers. After wavefield solution, $\mathcal{U}(\tau,\gamma,\omega)$, has been computed at all rayfield locations, the result is mapped to Cartesian coordinates using sinc-based interpolation operators in a neighborhood about each mapped point.

The chicken and the egg

The 2-D phase-ray extrapolation approach detailed above is analogous to the fabled 'chicken and egg' conundrum: which to compute first? Stated explicitly, phase-rays must be calculated from a known wavefield solution; however, the wavefield is itself the quantity being computed. Because the wavefield is not known *a priori*, clearly a new strategy is required to resolve these disparate observations.

There are (at least) two possible ways to circumvent this issue. The first procedure involves using precomputed wavefields to train the phase-ray coordinate system by: i) establishing the longer wavelength rayfield structure by raytracing in a background velocity model using a broadband solver; ii) calculating an initial monochromatic wavefield solution using the background rayfield as the coordinate system; iii) computing an updated ray-coordinate system from the previous wavefield solution; and iv) calculating an updated wavefield on the improved phase-ray coordinate system. This procedure is addressed in companion paper Shragge and Biondi (2004) in this report.

A second approach is to use wavefields parameterized in phase-ray coordinates, rather than Cartesian, to dictate the direction of the next rayfront step. For judiciously chosen $\Delta\tau$ steps, both the rayfield direction and resulting wavefield evolves slowly, and ray directions differ by only small, incremental amounts in a neighborhood of τ. Hence, the orientation of previous few ray steps provide a good estimate of the required ray direction at the present τ step. Thus, a phase-ray coordinate system may be computed on the fly using the magnitude of the wavefield phase gradient of the previous few steps and the local velocity function.

Using a wavefield parameterized in ray-coordinates to generate the underlying coordinate system requires that the governing phase-ray equations are transformed accordingly. Fortunately, the magnitude of a scalar field gradient remains invariant to coordinate transformation, and is related through a change of variables,

$$\frac{\partial \phi}{\partial x_l} = \frac{\partial \phi}{\partial y_m}\frac{\partial y_m}{\partial x_l}, \tag{11}$$

where $x_l = [x, z]$ and $y_m = [\tau, \gamma]$ are the Cartesian and ray coordinate basis, respectively, and l and m are dummy indices. This reparameterization leads to the ray-coordinate phase-ray equations,

$$\frac{\mathrm{d}r_i}{\mathrm{d}s} = \frac{\partial \phi}{\partial y_j}\frac{\partial y_j}{\partial x_i}\left[\left(\frac{\partial \phi}{\partial y_m}\frac{\partial y_m}{\partial x_l}\right)\left(\frac{\partial \phi}{\partial y_m}\frac{\partial y_m}{\partial x_l}\right)\right]^{-\frac{1}{2}}. \tag{12}$$

Equations (11) can be written explictly in Cartesian and ray variables,

$$\begin{bmatrix} \frac{\partial \phi}{\partial x} \\ \frac{\partial \phi}{\partial z} \end{bmatrix} = \begin{bmatrix} \frac{\partial \phi}{\partial \tau}\frac{\partial \tau}{\partial x} + \frac{\partial \phi}{\partial \gamma}\frac{\partial \gamma}{\partial x} \\ \frac{\partial \phi}{\partial \tau}\frac{\partial \tau}{\partial z} + \frac{\partial \phi}{\partial \gamma}\frac{\partial \gamma}{\partial z} \end{bmatrix}. \tag{13}$$

The partial derivatives between the two coordinate systems in equations (11) are directly related to traditional ray parameters. Cartesian derivatives of τ are the horizontal and vertical plane-wave slownesses, while those with respect to γ are the local rotation angle to the Cartesian coordinate system (illustrated in Figure 1). Explicitly, these functions are,

$$\begin{aligned} \frac{\partial \tau}{\partial x} &= \frac{\sin\theta}{v(\mathbf{x})}, \qquad \frac{\partial \tau}{\partial z} = \frac{\cos\theta}{v(\mathbf{x})}, \\ \frac{\partial \gamma}{\partial x} &= \cos\theta, \qquad \frac{\partial \gamma}{\partial z} = \sin\theta, \end{aligned} \tag{14}$$

where parameter θ is the angle formed between a ray and the z-axis (assumed to be positive downward).

Computing a weighted average direction from the previous M steps requires saving $M+1$ previous wavefield steps. The discrete version of equation (12) for ray step at index t, Δr_i^t, is,

$$\Delta r_i^t \approx v(r_i(\mathbf{x}))\,\Delta\tau \sum_{m=1}^{M} \beta_m \frac{\Delta r_i^{t-m}}{\Delta s^{t-m}}, \tag{15}$$

where Δs^t is the scalar step magnitude at step t, and β_m are a set of weights subject to,

$$\sum_{m=1}^{M} \beta_m = 1. \tag{16}$$

Weights β_m may be chosen to yield a spline fit of at least second-order accuracy.

The use of previous wavefield solutions to compute solutions to equations (12) naturally gives rise to a broadened finite difference stencil. Figure 2 presents the finite difference stencil for the M=2 case that has second-order accuracy in γ and τ.

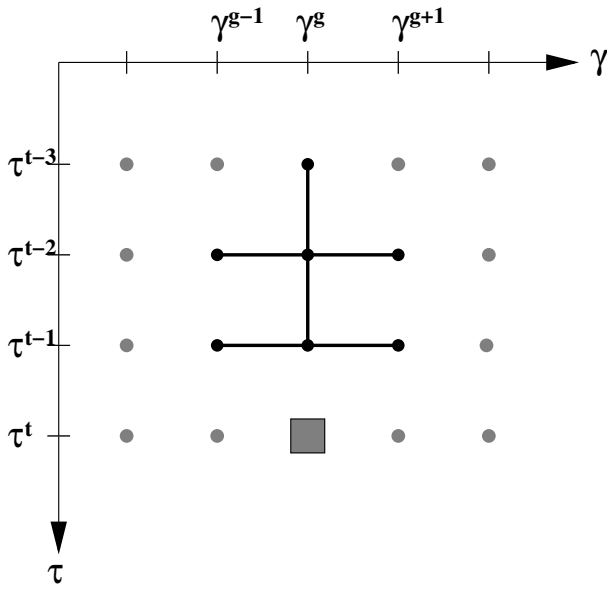

Figure 2: Finite difference stencil for calculating wavefield solution at present step using the previous two steps (M=2). The solid square represents the location of the desired rayfield solution, and the in-filled circles connected by lines are the points contributing to the solution point. jeff1-stencil [NR]

Bootstrapping the chicken to get the egg

Having parameterized the phase-ray equations in ray-coordinates, and specified a method for updating rayfront directions, it is possible to detail the bootstrap method that forms the core of adaptive phase-ray extrapolation procedure. Figure 3 presents a flowchart representation of the bootstrap procedure. Rayfields must be computed prior to wavefield extrapolation.

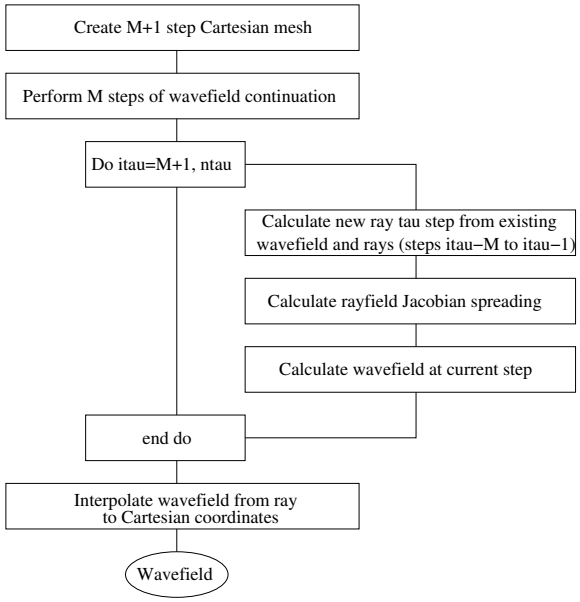

Figure 3: Flow chart of the bootstrap procedure jeff1-flow [NR]

Accordingly, the coordinate system is first initialized by assuming the first $M+1$ steps using an educated guess of where wavefront energy will propagate. Two examples are an expanding circular mesh for a point source (illustrated in Figure 1) or a tilted coordinate system for a dipping plane-wave source (illustrated in Figure 4). After coordinate system initialization, M wavefield extrapolation steps are carried out to generate the required $M+1$ step wavefield.

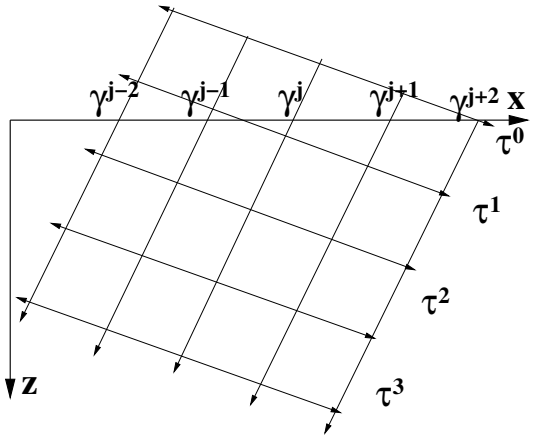

Figure 4: The first 4 steps of an initial coordinate mesh appropriate for initializing a dipping plane-wave source. At coordinate locations above the ground surface the velocity model is assumed to be constant so that extrapolated energy enters the model as a monochromatic plane-wave (i.e. in both ω and k_x). jeff1-dipstart [NR]

The bootstrap process is a loop around three separate calculations: i) ray step Δr_i from the previous M wavefield steps; ii) rayfield Jacobian spreading, J, and associated functions; and iii) wavefield $\mathcal{U}$ at the current step. The final step involves interpolating the wavefield from the ray to the Cartesian coordinate basis, and is done independently after extrapolation.

PHASE-RAY EXTRAPOLATION EXAMPLES

In this section we illustrate the utility of adaptive phase-ray wavefield extrapolation using 2-D synthetic examples involving progressively more complex velocity models. Underlying ray-coordinate systems were calculated according to equation (12), and wavefields were extrapolated on the computed rayfields using the ray-coordinate 15° equation (equation (9)). All images were computed using uniform time steps with individual $\Delta\tau$ dependent on velocity model complexity. Orthogonal coordinate γ was parameterized as either a punctual or a plane wave source. Point source images required a parameterization of γ over shooting angle starting at radius, R. The initial 4-step coordinate mesh was created from a circularly expanding rayfront with an angular range bounded by γ_{min} and γ_{max}. Initial wavefields consisted of constant amplitude lines separated in τ and distributed uniformly over coordinate γ. Plane-wave images required a parameterization of γ over surface coordinate x_o. The initial 4-step coordinate system was a Cartesian mesh tilted at the dip angle of the plane-wave being extrapolated. Initial wavefields again consisted of constant amplitude lines separated in τ and distributed uniformly over surface position, x_o.

We designed the first extrapolation example to test the method on a smooth velocity function of sufficient contrast to enable overturning waves. The velocity model, shown in the left panel of Figure 5, consists of a broad Gaussian velocity anomaly that is 86% slower than the background velocity of 3000m/s. Superposed on the Gaussian anomaly are vertical and horizontal gradients of 0.1 and -0.05 s^{-1}, respectively. The first test involved using a point source located at 3000m. Rays were computed between $-60°$ and $60°$ assuming an initial radius of 200m. Phase-ray wavefield extrapolation was then carried out with a constant $\Delta\tau$ spacing of 0.0005s at a 5Hz frequency. The resulting ray-coordinate system, superposed on the left panel of Figure 5, is smooth and triplication-free. The middle panel presents the corresponding 5Hz

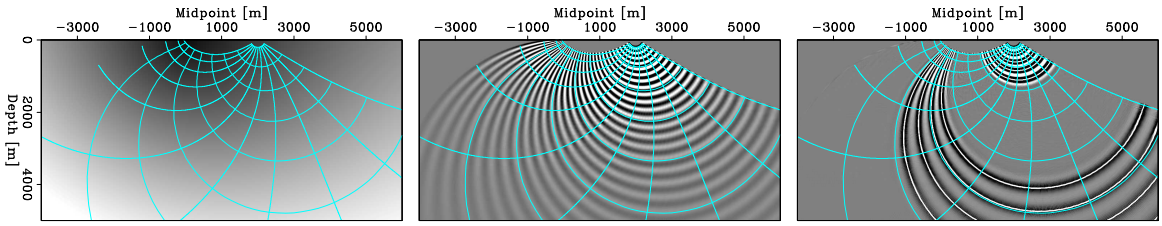

Figure 5: Point source wavefield extrapolation example. Left: Velocity model with Gaussian-shaped anomaly 86% slower than the background velocity of 3000m/s. Superposed over top are vertical and horizontal gradients of 0.1 and -0.05km/s per km, respectively, and the 5 Hz ray-coordinate system. Middle: The 5Hz monochromatic wavefield. Right: Broadband wavefield calculated using a 0.2-25Hz frequency band. jeff1-Circle.ps [CR]

monochromatic wavefield interpolated from the ray-coordinate system to a Cartesian mesh of spacing $\Delta x = \Delta z = 10$m. These two panels illustrate that both the rayfield and wavefield successfully overturn. Wavefield wavelengths are observed to compress in the region of slow velocity about the Gaussian anomaly, and to expand at greater depths. The right panel presents the broadband image constructed for frequencies between 2-35Hz. All wavefield frequencies were extrapolated on a stationary 5Hz ray coordinate system.

The second example, shown in Figure 6, is the plane-wave equivalent to Figure 5. The panels in Figure 6 are similar to those presented in the previous figure. The initial coordinate

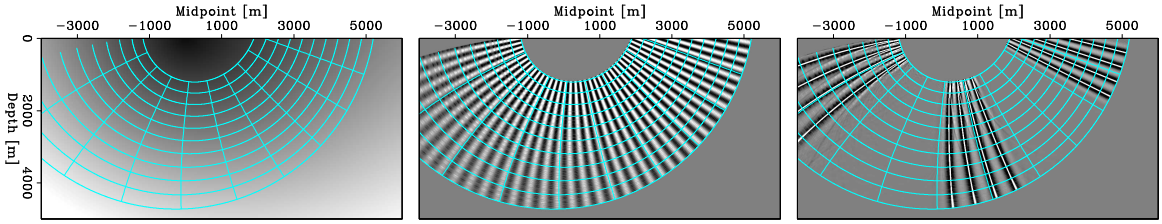

Figure 6: Extrapolation example for plane-wave with -10° dip. Left: Velocity model consisting of a Gaussian-shaped anomaly 86% slower than the background velocity of 3000m/s. Superposed are vertical and horizontal gradients of 0.1 and -0.05km/s per km, and the calculated 5Hz ray-coordinate system. Middle: The 5Hz monochromatic wavefield. Right: Broadband image calculated using a 0.2-25Hz frequency band. jeff1-Circle.pw [CR]

system and wavefield tilt angle was -10°, and the spacing between individual rays was set at 20m. The left and middle panels show the 5Hz rayfield and the corresponding 5Hz wavefield, respectively. Again, the rayfield is observed to compress along coordinate γ as it nears the center of the Gaussian anomaly leading to increased amplitudes and shorter wavelengths. The right panel presents the broadband wavefield calculated in the 0.2-25Hz frequency band. Again, all wavefield frequencies were extrapolated on a stationary 5Hz ray-coordinate system. As in the previous figure, the broadband result overturns and is triplication-free.

The next example demonstrates adaptive phase-ray wavefield extrapolation in a Gulf of Mexico salt model. The background velocity of the model, shown in the left panel of Figure 7,

is a typical Gulf of Mexico v(z) velocity gradient. The superposed salt body is characterized

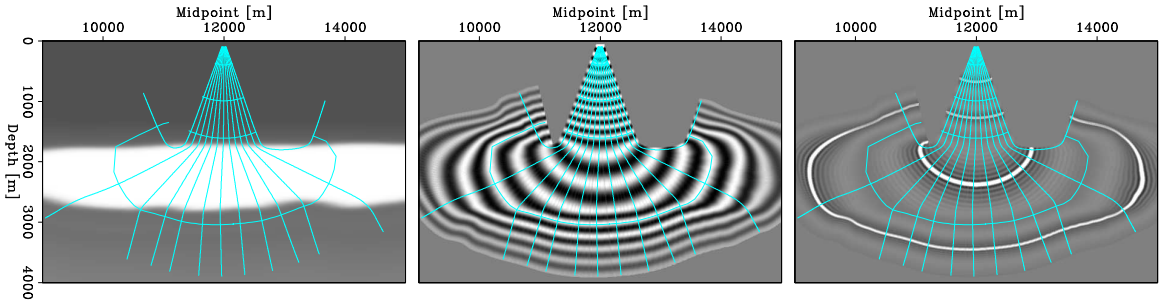

Figure 7: Point source extrapolated in a typical Gulf of Mexico velocity model. Left: Salt velocity model consisting of a typical Gulf of Mexico v(z) velocity gradient, with a salt body of 4700m/s wavespeed superposed at depth, and the calculated 5Hz monochromatic rayfield. Middle: The 5Hz monochromatic wavefield derived. Right: Broadband image computed for the 2-35Hz frequency band. jeff1-Salt.ps [CR]

by a higher wavespeed (4700m/s) and a somewhat rugose bottom of salt interface. A point source was modeled at surface position 12000m with a starting radius of 200m. The initial angular coverage was bounded by $\gamma_{min} = -22^\circ$ and $\gamma_{max} = 20^\circ$ because shooting beyond this angular range lead to ray-coordinate triplication. The superposed rayfield in the left panel demonstrates the effect of strong velocity contrasts and a rugose interface between the bottom of salt body and the enveloping sediments. At angles tending away from vertical (i.e. θ=0), rays increasingly refract in accordance with Snell's law, become horizontal, impinge on the salt-sediment interface, and eventually refract upward at fairly steep angles. The middle and right panels present the 5Hz monochromatic and 2-35Hz broadband wavefields, respectively. Again, the ray-coordinate system in the right panel was assumed to be stationary, and all frequencies were extrapolation on 5Hz rayfield.

RAY-COORDINATE TRIPLICATION

The phase-ray extrapolation examples discussed so far have intentionally avoided triplicating wavefields. However, wavefield triplications are commonly observed in seismic data, especially in areas of complex geology where the phase-ray extrapolation technique shows most potential. In this formulation, the ray coordinate system is computed from previous wavefield steps; hence, the underlying basis will begin to triplicate immediately after the wavefield does. Thus, a contingency plan must exist to prevent numerical instabilities associated with coordinate triplication.

Wavefield triplication naturally occurs when a propagating wavefield is focused by lateral velocity variation acting as an optic lens. One canonical example is a Gaussian-shaped slow velocity anomaly, where continued wavefields exhibit a characteristic bow-tie signature beneath the anomaly. Numerical instabilities occur when calculating the ray coordinate system in the vicinity of the bow-tie because neighboring rays overlap while following their respective branches of the bow-tie. At the crossing point, the Jacobian in equation (8) is identically

zero leading to infinite values of wavenumber k_τ in equation (6). Infinite wavenumbers, of course, are not realizable in practice and are only a theoretical artifice of the wavefield being multivalued at that point. Accordingly, instabilities with ray coordinate triplication may be rectified through an appropriate accounting for the wavefield's multivalued nature during numerical calculations.

One way to deal with multivalued functions is to treat the individual branches of the triplication bow-tie as independent wavefield components that should be held incommunicado. This idea, borrowed from ideas in the mathematical field of complex analysis (Cohn, 1967), is illustrated in Figure 8. Isolating triplication branches requires computing the locations of wavefield

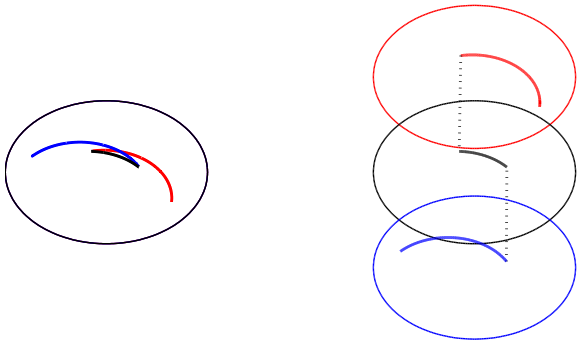

Figure 8: Cartoon of our methodology of splitting different branches of a triplication. Left: Triplication where the 3 branches lie on the same plane; Right: Same triplication as in left panel, but with each branch residing on a separate plane. Our method is to effectively restrict communication between branches when calculating derivatives and other associated quantities. jeff1-branch [NR]

triplications from crossing ray segments in the rayfield. In 2-D, crossing ray segments may be identified by modeling the segments as infinite lines, computing their intersection point, and testing whether this location falls within the area bounded by the ray segments. Where this test reveals a crossing point (or branch point), the rayfield has triplicated and should be cut into individual branches. Jacobian coordinate and other related functions that require the computation of derivatives, can be then be calculated on their respective branches (i.e. on one of the three planes in Figure 8). For locations not on branch cuts, centered finite-difference stencils may be used; however, at branch-cut locations appropriate left- and right-sided derivatives are required. Importantly, the locations of branch cuts are kept for all subsequent computations. Finally, we acknowledge that this treatment of rayfield triplication is cursory and remains a topic of ongoing research. However, similarities between our proposed method for handling coordinate triplications and the standard branch cut technique of complex analysis should provide us with a powerful set of tools for further development.

The canonical example of a slow Gaussian-shaped velocity anomaly is presented in Figure 9. The velocity model used in this example is presented in the left panel, and consists of a slow Gaussian anomaly of maximum -50% perturbation of the 2000m/s background velocity. The 10Hz phase-ray coordinate system is also overlain. The middle panel shows the 10Hz wavefield. The hatched pattern in the lower center of the figure is created by the superposition of the phases of the two competing triplication branches (as discussed in Shragge and Biondi (2003)). The right panel presents the broadband result (0.1-30Hz) computed on a stationary 10Hz phase-ray coordinate system. In the lower part of the figure, the signature bow-ties of the

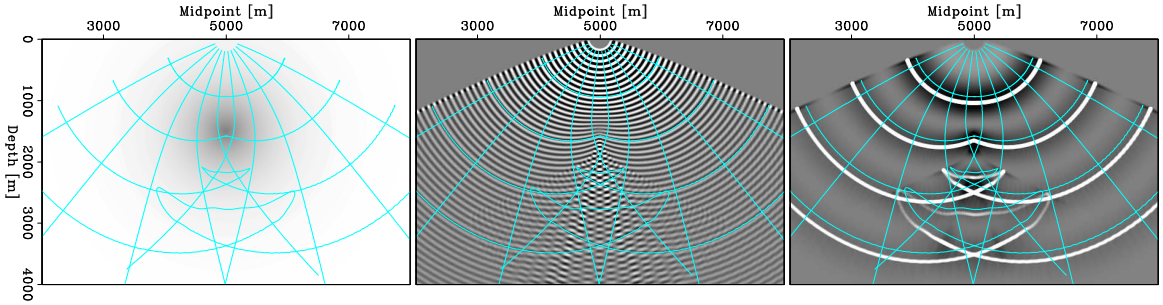

Figure 9: Canonical example of a slow Gaussian velocity perturbation. Left: model with background velocity 2000m/s on which is superposed a slow Gaussian of -50% of the background velocity, and the 10Hz coordinate system. Middle: 10Hz monochromatic image. Right: broadband (0.1-30Hz) wavefield calculated using a stationary 10Hz ray coordinate system. jeff1-Gauss.ps [CR]

triplicating wavefield are evident. The slight undulations on the centered part of the bow-tie, though, should not be present. Our conjecture is that these are an artifact of coordinate system interpolation.

CONCLUSIONS

We demonstrate the utility of a ray-based Riemannian wavefield extrapolation method using an adaptive bootstrap approach to calculate the ray-coordinate system directly from the wavefield. This bootstrap procedure allows for frequency-dependent ray-coordinate systems to be computed on-the-fly from the wavefield phase gradient and the velocity model. Coupling this procedure with RWE leads to a general frequency-dependent extrapolation procedure capable of following a wavefront as it propagates, overturns, and even triplicates. We propose that in locations where the ray-coordinate system triplicates, the Jacobian spreading and other required functions may be calculated by cutting the triplication into its constituent branches and using appropriate one-sided finite difference stencils. The full proof of this conjecture, though, remains a topic of future research.

ACKNOWLEDGMENTS

We acknowledge Western Geco for permission to use the Gulf of Mexico velocity model. We thank Biondo Biondi and Sergey Fomel for helpful discussions.

REFERENCES

Albertin, U., Yingst, D., and Jaramillo, H., 2001, Comparing common-offset Maslov, Gaussian beam, and coherent state migrations: Soc. of Expl. Geophys., Expanded Abstracts, 913–916.

Brandsberg-Dahl, S., and Etgen, J., 2003, Beam-wave imaging: Soc. of Expl. Geophys., Expanded Abstracts, 977–980.

Claerbout, J., 1985, Imaging the earth's interior: Stanford University.

Cohn, H., 1967, Conformal mapping on Riemann surfaces: Dover Publications, Inc., New York.

de Hoop, M. V., Le Rousseau, J., and Wu, R. S., 2000, Generalization of the phase-screen approximation for the scattering of acoustic waves: Wave Motion, **43-70**.

Etgen, J., 2002, Waves, beams and dimensions: an illuminating if incoherent view of the future of migration: Soc. of Expl. Geophys., invited presentation.

Fomel, S., 2003, Angle-domain seismic imaging and the oriented wave equation: Soc. of Expl. Geophys., Expanded Abstracts, 893–898.

Foreman, T. L., 1989, An exact ray theoretical formulation of the Helmholtz equation: J. Acoust. Soc. Am., **86**, 234–246.

Gazdag, J., 1978, Wave equation migration with the phase-shift method: Geophysics, **43**, 1342–1351.

Gray, S., Notfors, C., and Bleistein, N., 2002, Imaging using multi-arrivals: Gaussian beams or multi-arrival Kirchhoff?: Soc. of Expl. Geophys., Expanded Abstracts, 1117–1120.

Guggenheimer, H., 1977, Differential geometry: Dover Publications, Inc., New York.

Hill, N. R., 2001, Prestack Gaussian-beam depth migration: Geophysics, **66**, no. 4, 1240–1250.

Ristow, D., and Ruhl, T., 1994, Fourier finite-difference migration: Geophysics, **59**, no. 12, 1882–1893.

Sava, P., and Fomel, S., 2001, 3-D traveltime computation using Huygens wavefront tracing: Geophysics, **66**, no. 3, 883–889.

Sava, P., and Fomel, S., 2003, Seismic imaging using Riemannian wavefield extrapolation: SEP–**114**, 1–30.

Sava, P., and Fomel, S., 2004, Wavefield extrapolation in Riemannian coordinates: Soc. of Expl. Geophys., Expanded Abstracts.

Shan, G., and Biondi, B., 2004, Imaging overturned waves by plane-wave migration in tilted coordinates: SEP–**115**, 1–12.

Shragge, J., and Biondi, B., 2003, Wavefield extrapolation in phase-ray coordinates: SEP–**114**, 31–44.

Shragge, J., and Biondi, B., 2004, Phase-ray coordinate system updating: SEP–**115**, 29–38.

Červený, V., 2001, Seismic ray theory: Cambridge Univ. Press.

Zhang, J., and McMechan, G. A., 1997, Turning wave migration by horizontal extrapolation: Geophysics, **62**, no. 01, 291–297.